Journal of Magnetic Resonance 212 (2011) 47–54

Contents lists available at ScienceDirect

Journal of Magnetic Resonance

journal homepage: www.elsevier.com/locate/jmr

Monitoring mass transport in heterogeneously catalyzed reactions by field-gradient NMR for assessing reaction efficiency in a single pellet

L. Buljubasich [a], B. Blümich [a], S. Stapf [b,*]

[a] Inst. of Technical Chemistry and Macromolecular Chemistry ITMC, RWTH Aachen, D-52074 Aachen, Germany
[b] Dept. of Technical Physics II, TU Ilmenau, PO Box 100565, D-98684 Ilmenau, Germany

ARTICLE INFO

Article history:
Received 28 April 2011
Revised 8 June 2011
Available online 16 June 2011

Keywords:
PGSE NMR
NMR diffusometry
Flow NMR
Heterogeneous catalysis
Chemical engineering
Reaction engineering

ABSTRACT

An important aspect in assessing the performance of a catalytically active reactor is the accessibility of the reactive sites inside the individual pellets, and the mass transfer of reactants and products to and from these sites. Optimal design often requires a suitable combination of micro- and macropores in order to facilitate mass transport inside the pellet. In an exothermic reaction, fluid exchange between the pellet and the surrounding medium is enhanced by convection, and often by the occurrence of gas bubbles. Determining mass flow in the vicinity of a pellet thus represents a parameter for quantifying the reaction efficiency and its dependence on time or external reaction conditions. Field gradient Nuclear Magnetic Resonance (NMR) methods are suggested as a tool for providing parameters sensitive to this mass flow in a contact-free and non-invasive way. For the example of bubble-forming hydrogen peroxide decomposition in an alumina pellet, the dependence of the mean-squared displacement of fluid molecules on spatial direction, observation time and reaction time is presented, and multi-pulse techniques are employed in order to separate molecular displacements from coherent and incoherent motion on the timescale of the experiment. The reaction progress is followed until the complete decomposition of H_2O_2.

1. Introduction

Heterogeneous catalytic reactions, where the catalysts consists of a porous pellet (usually supported by the inclusion of metallic species such as Ni, Pt, Pd, Co and Cu) is one of the most important applications of porous media in Chemical Engineering. Since in that type of reactions the solid catalyst surface is responsible for catalytic activity, a large readily accessible surface in easily handled materials is desirable. By a variety of methods, active surface areas of the order of 1000 m^2 per gram of catalyst can be obtained.

These reactions play an important role in many industrial processes, such as the production of methanol, sulfuric acid, ammonia, and various petrochemicals, polymers, paints and plastics. It is estimated that well over 50% of all the chemicals produced today are made with the use of catalysts [1].

The rate constants of the heterogeneous catalytic reactions, and therefore the efficiency of the reaction, depends on the local environment of the catalyst surface including concentration and distribution of reagents and of possible deactivating substances in the vicinity of the active sites, as well as on the rate of molecular transport as influenced by the topology and pore space geometry [2]. Therefore, the development and optimization of the catalyst becomes an important part of the design of a chemical process, and is subject to extensive research and investment. For that purpose, flexible testing methods to quantify the dependence of the reaction parameters on variables introduced in the design of different catalyst are of invaluable help. Among the methods that can be used for evaluating and assessing catalysts, NMR is perhaps the ultimate technique because it provides a rich toolbox for the investigation of properties on all length scales of interest while remaining strictly non-invasive.

From the NMR point of view, the motivation to apply the technique to small-scale reaction units is two-fold. First, the investigation of full-scale chemical reactors used in production may be impossible due to the size or cost restriction of the hardware, or in case of NMR Imaging, may be feasible but only for an insufficient spatial resolution of the system, typically being of the order of one-hundredth of the resonator dimension. On the other hand, in order to follow reactions at the level of the actual reaction sites, studies of a single catalyst pellet at well-defined conditions can be performed with a much higher spatial resolution, permitting the verification and discrimination of coupled diffusion/reaction models. The second reason is more hardware-related, and exploits the superior performance of gradient and radiofrequency detectors on small scales, leading to the improved spatial and temporal resolution that are required to understand processes which are intrinsically fast or are localized to the submillimeter scale, such as

* Corresponding author. Fax: +49 03677 69 3770.
E-mail address: siegfried.stapf@tu-ilmenau.de (S. Stapf).

1090-7807/$ - see front matter © 2011 Elsevier Inc. All rights reserved.
doi:10.1016/j.jmr.2011.06.007

transport dominated by self-diffusion [3]. In addition, the studies on small-scale reactors is of particular interest for the catalyst developers, because it makes the design-testing iteration relatively easy to perform, without much hardware requirement.

The efficiency of a single pellet reactor can be monitored in two ways, either by observing characteristic properties of the pellet interior such as the liquids relaxation times and diffusion coefficients, or by quantifying the increased mass transport in the exterior volume which is expected from exothermic reactions, but is enhanced significantly more if the reaction involves the generation of gas bubbles. While distortions of the magnetic field inside the pellets do, in general, not allow chemical resolution and render imaging difficult due to short relaxation times, the result of reactions, however, manifests itself in convection outside of the pellet that can easily be picked up by diffusion- or velocity encoding pulse sequences. Mass transfer outside of the single pellet will, in turn, affect overall transport of reactants and heat within a reactor column [4].

In order to demonstrate the feasibility of using the time dependence of the so called effective diffusion coefficients for monitoring heterogeneously catalysed reactions in the vicinity of the pellet, and then probing different aspects of the catalyst particles, the decomposition of hydrogen peroxide,

$$2H_2O_2(\text{liquid}) \rightarrow 2H_2O + O_2(\text{gas}) \quad (1)$$

is considered as a standard example for a gas-forming reaction. The decomposition, which is almost absent in the bulk liquid, is considerably enhanced in the presence of Cu- and Pt-doped commercial Al_2O_3 porous catalyst particles [5].

In this study, the temporal evolution of vertical and horizontal effective diffusion coefficients, as indicators of the reaction's status, were monitored up to the full conversion of a defined amount of H_2O_2.

2. Dynamics during the reaction

In most reactions of technical interest, one of the involved components is in the gas phase. The gas generated during the reaction, predominantly in the vicinity of the metal sites at the pore surface, is first dissolved within the surrounding liquid phase until the maximum solubility is exceeded. The formation of a gas phase, however, depends on the interface tension and the size and tortuosity of the pore system. The bubbles might therefore be generated inside large pores, or might only form at the external surface of the pellet. In general, each pore generates bubbles at a certain rate or frequency: large pores lead to large bubbles at low frequency, and *vice versa*. For a constant reaction rate, these properties can be predicted for isolated pores [6]. In a real catalyst pellet, however, the coupling of all the pores within the interconnected pore space gives rise to a pattern of bubble generation that cannot be computed analytically [7].

The production and motion of gas bubbles results in a random change in the velocities of the liquid surrounding the pellet. The liquid molecules (H_2O_2 and H_2O in this particular case) are displaced and driven by the rising bubbles. The higher the production of gas, the larger the amount of bubbles will be. The bubbles, eventually rising upwards, produce an increased mean-squared displacement of the liquid's molecules along z- compared to x-direction. This enhances the mass transport in the vicinity of the pellet, and, in consequence, the rate of reaction. Fig. 1 shows the situation schematically.

The rate of oxygen generation and bubble production depends on the reactant concentration. A decrease in the mean-square displacement is then expected as the reaction proceeds.

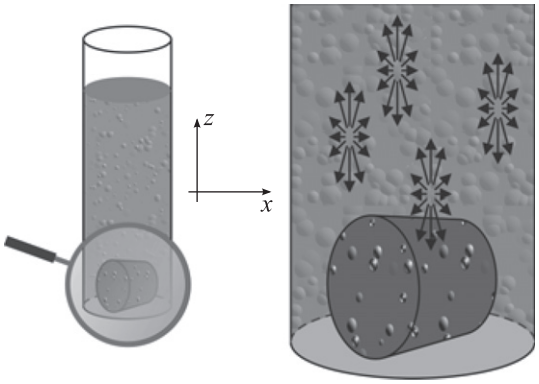

Fig. 1. Layout used in the experiments. A magnification of the vicinity of the pellet is shown on the right hand figure with a representation of the liquid's molecules displacements.

3. Reaction evolution and effective diffusion coefficients

In an PGSTE NMR experiment, where the spins are subjected to a spatially dependent magnetic field, the liquid's molecules moving in the presence of a magnetic field gradient accumulate a net phase. The echo signal, $E_{\Delta}(\mathbf{q}) = \int_{-\infty}^{\infty} \overline{P}(\mathbf{R}, \Delta) \exp[i2\pi\mathbf{q}\cdot\mathbf{R}]d\mathbf{R}$, is a superposition of transverse magnetizations in which each phase term is weighted by the probability for a spin to be displaced by $\mathbf{R}$ in the time interval between gradient pulses Δ. The vector $\mathbf{q}$ is defined as $\mathbf{q} = (2\pi)^{-1}\gamma\mathbf{g}\delta$, where $\mathbf{g}$ is the gradient strength and δ is the gradient pulse duration [8]. Fourier transformation of the echo signal with respect to $\mathbf{q}$ returns the average propagator [9] for the nuclear spin displacement, $\overline{P} = (\mathbf{R}, \Delta)$.

In its original conception, the PGSE (or PGSTE) NMR experiment was used to measure molecular self-diffusion in confinement, for which the average propagator is either a Gaussian function or deviates from a Gaussian in a defined fashion. In a more general interpretation, the 1-D average propagator represents the probability that a molecule starting at any position within the sample, is displaced by a distance Z (in case of z-direction) during the observation time Δ. In that interval, the averaged velocity $v_z = Z/\Delta$ can be defined, and the average propagator becomes a velocity probability function. Valuable information about the system can be extracted, in many cases, from the propagator's shape in different directions. For instance, anisotropic self-diffusion is a well-established methodology in medical imaging [10], whereas flow of fluids through porous systems [11,12], convective flow in single drops [13], or motion in particle systems [14] have been characterised by the shape of the propagator in orthogonal directions.

Although the propagator represents a relatively standard technique when applied to study fluid dynamics, it possesses some disadvantages when is applied to monitor a reaction, mainly because the information about the reaction evolution is not easily quantifiable from the evolution of propagator shapes. In turn, there are some advantages on measuring parameters directly from the q-space data. In case of molecular self-diffusion, the echo attenuation can be calculated, for the PGSTE NMR experiment, from the well known Stejskal–Tanner relation [15]. The self-diffusion coefficient is then derived from the slope of semilogarithmic plots of E versus $\gamma^2 g^2\ \delta^2(\Delta - \delta/3)$. On the other hand, in the case of uniform (plug) flow, with a constant velocity component $\mathbf{v}$ along the direction $\mathbf{q}$, there is a modulation of the phase of the echo function, with no net signal attenuation. Fourier transforming the q-space data yields a propagator for motion, which may provide an intuitive way of representing the physics of a system. The process of Fourier transforming data may, however, induce ringing artifacts if the data are truncated before the signal has dropped below the noise level of the experiment. For this reason the data must be collected over a

wide range of q-space. For many cases, such detailed sampling is unnecessary, as the important features of a propagator can be determined readily from a few low q-space data points without subsequent Fourier transformation, reducing the necessary gradient strength and the experimental time [16].

The echo attenuation function described above represents the ensemble-averaged phase shift, $\overline{\exp[i2\pi\mathbf{q}\cdot\mathbf{R}]}$. This expression can be expanded into a Taylor series,

$$E_{\Delta}(\mathbf{q}) \approx 1 - (1/2!)(2\pi q)^2\overline{Z^2} + (1/4!)(2\pi q)^4\overline{Z^4} \quad (2)$$

where Z is the component of displacement along the gradient direction defined by q. Eq. (2) is useful, since it tells us that whatever the shape of the propagator function, $\overline{P}(Z,\Delta)$, the initial decay of $E(q,\Delta)$ with respect to q will always yield the ensemble-averaged mean square displacement $\overline{Z^2}$. An effective diffusion (or dispersion) coefficient, $D_{\text{eff}} = \overline{Z^2}/2\Delta$, can be associated with it [16]. In this work, we restrict the discussion of the results on a comparison of effective diffusion coefficients.

Self diffusion in simple liquids represents a good example of randomly directed motion with rapid fluctuations. Typical correlation lengths are on the order of 10^{-10} m, with corresponding correlation times much shorter than the inverse of the Larmor frequency. Nevertheless, small molecular stochastic motions can exist at different scales. A familiar example could be a fluid experiencing a turbulent flow.

Moving the focus to micro-structural scale, irregular motion is a feature of flow through porous media or biological tissue. In those cases the molecules follow paths which are randomly directed, mainly due to the complexity of the pore and channel distributions. Fluctuations in the motion may occur either due to the random orientation of the channels and capillaries, or because of path divergence at branch points, where because of the chaotic character of the motion, small changes in the initial conditions can lead to markedly different final directions. This type of incoherent motion is sometimes called perfusion.

We will separate here the random flow regime into two regimes. In the first, called *stationary random flow*, the molecular motions are randomly distributed in magnitude and/or orientation, and represented by a time independent velocity field $\eta(\mathbf{u},\mathbf{r})$. Typical examples of this kind of motion are laminar flow in shear and flow in an array of randomly directed capillaries. Such situation is illustrated in Fig. 2A. In the second case, named *pseudodiffusion*, the molecular velocities are randomly distributed and also present a temporal fluctuation. Turbulence and branched capillary motion are examples of this kind of motion, schematically presented in Fig. 2B [8].

As a general model, we will consider the liquid as consisting of regions labelled by the index i (in the following, we use the convention introduced in [8]). The vector $\mathbf{v}$ describes the global mean velocity of the molecules, whereas $\mathbf{u}_i$ indicates the local mean velocity the ith region of the liquid. This motion has a typical ballistic character, with the correlation time τ_c^u and the corresponding correlation length $L_u \sim (\overline{\mathbf{u}^2})^{1/2}\tau_c^u$. Within every region labelled by index i the individual molecules, labelled by index j, undergo stochastic motion $\mathbf{r}_j$ due to self-diffusion. This motion has associated with it a correlation time τ_c^r and a correlation length $L_r \sim (D\,\tau_c^r)^{1/2}$. The three types of motion are, by this model, separated in correlation length and time, and then they can be treated as stochastically independent. Fig. 2C shows this model in detail.

The total displacement of a molecule labelled by j in the fluid element with index i is

$$\mathbf{r}_{ij}(t) = \mathbf{v}t + \mathbf{u}_i t + \mathbf{r}_j(t) \quad (3)$$

Let us assume that the system is observed for a time, say t_{obs}. If t_{obs} is long compared with the molecular self-diffusion correlation time but short compared with correlation time of the mean motion in every region, i.e. $\tau_c^r \ll t_{\text{obs}} \ll \tau_c^u$, the ensemble average of the molecules labelled by j over the observation time gives $\mathbf{r}_i = (\mathbf{v} + \mathbf{u}_i)t_{\text{obs}}$. If, on the other hand, t_{obs} is longer compared to the correlation time of the mean motion in the regions i, $\tau_c^u \ll t_{\text{obs}}$, the average over i gives $\mathrm{r} = \mathbf{v}t_{\text{obs}}$. We are interested in evaluating the PGSTE experiment in the stationary random flow regime, $\tau_c^r \ll t_{\text{obs}} \ll \tau_c^u$, where $\mathbf{u}_i$ is time independent. In the NMR experiment, t_{obs} is equivalent to the observation time Δ.

The PGSTE phase shift for a spin being located in the molecule with the indices ij is,

$$\phi_{ij}(t) = \gamma\int_0^t t'\mathbf{g}^*(t')\cdot(\mathbf{v}+\mathbf{u}_i)dt' + \gamma\int_0^t \mathbf{g}^*(t')\cdot\mathbf{r}_j(t')dt' \quad (4)$$

where $\mathbf{g}^*$ represents the effective gradient, which takes into account the radiofrequency pulses used in the sequence (see experimental section). The separability of the averages over i and j indicates that diffusion and random flow are uncorrelated. Thus, the total signal decay averaged over the liquid can be calculated separately, resulting in one factor representing the usual diffusive attenuation, and a second factor that resembles that usually associated with flow, but dealing with *fluctuating flow*. This latter factor is separable into a phase shift due to net flow and a term due to stationary random flow. By defining $\mathbf{p} = \gamma\int_0^t t'\mathbf{g}^*(t')dt'$, usually called 1st moment of gradient, we write this factor as $\exp(i\mathbf{p}\cdot\mathbf{v})\overline{\exp(\mathbf{p}\cdot\mathbf{u}_i)}$. For the PGSTE sequence (Fig. 3A) the echo attenuation becomes,

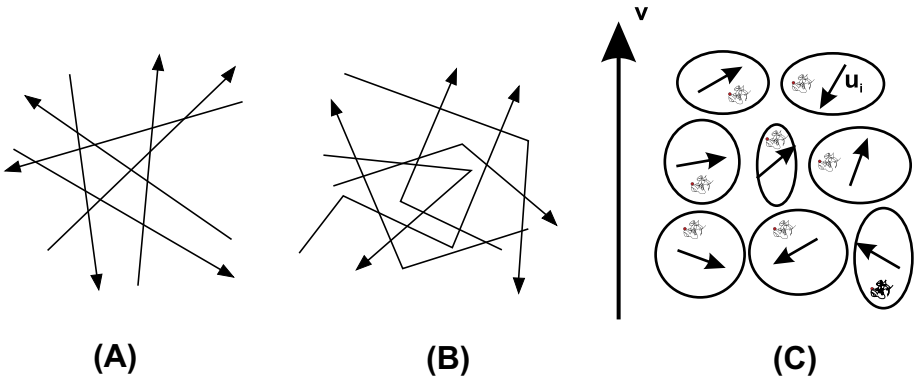

Fig. 2. (A) A representation of stationary random flow. The molecules move in randomly distributed directions, and the motion is describable by a time-independent velocity field. (B) Example of pseudodiffusion. Flow occurs in branched capillaries and the velocity direction fluctuates with a correlation time of the order of the ratio of the mean branch separation to the mean velocity. (C) General model for the liquid molecules. It consists of regions labelled by the index i, with an associated internal constant velocity $\mathbf{u}_i$. The regions are superimposed onto a mean velocity $\mathbf{v}$ common to all of them. Within the region with index i the individual molecules, labelled with the index j, experience stochastic motion $\mathbf{r}_j$ due to self-diffusion.

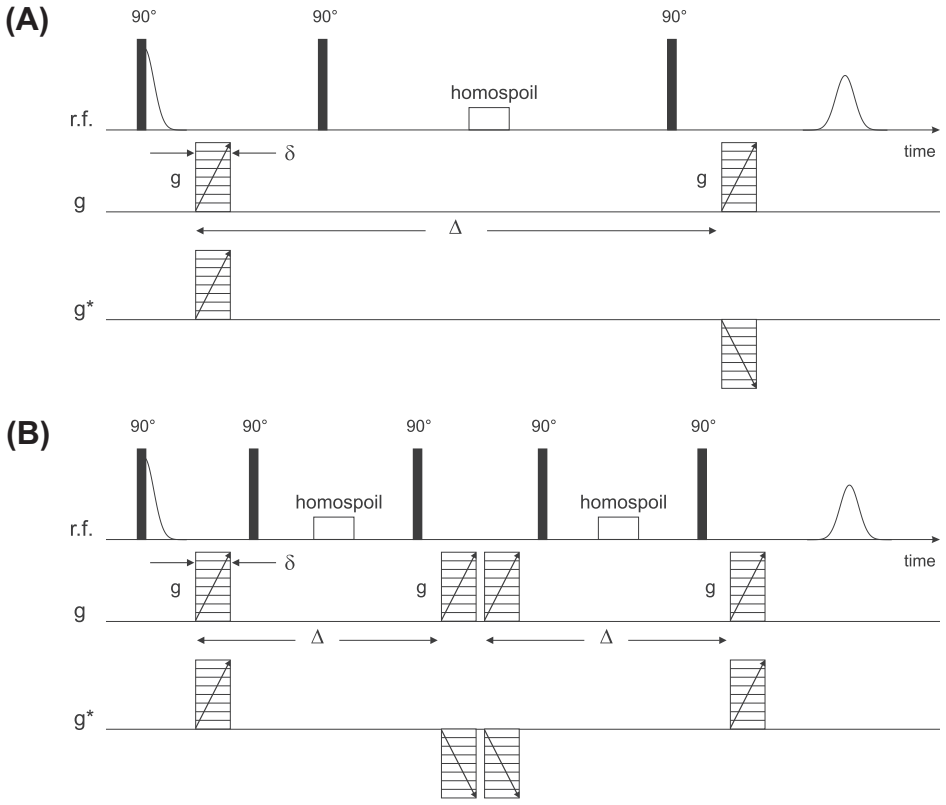

Fig. 3. Pulse Gradient Stimulated Echo sequences used in the experiments. (A) PGSTE and (B) Double PGSTE.

$$E(\mathbf{g}) = \exp(i\gamma\delta\mathbf{g}\cdot\mathbf{v}\Delta)\overline{\exp(\mathbf{p}\cdot\mathbf{u}_i)}\exp[-\gamma^2\delta^2 g^2 D(\Delta-\delta/3)) \quad (5)$$

The stationary random flow factor $\overline{\exp(\mathbf{p}\cdot\mathbf{u}_i)}$ can be evaluated by assuming that the direction of **u** is random over the position **r**. In the case of PGSTE the exponent becomes $(1/6)\overline{u^2}\gamma^2 g^2\delta^2\Delta^2$[17]. By comparing with the echo attenuation due to self-diffusion, an effective diffusion coefficient can be defined in this case by

$$D_{\text{eff}} = \frac{1}{6}\overline{u^2}\Delta \quad (6)$$

Stationary random flow is identified by a specific signature in a PGSTE experiment: the echo is attenuated similar to diffusion but with an effective diffusion coefficient proportional to the observation time Δ. On the other hand, for the Double PGSTE (Fig. 3B), which is usually referred to as velocity compensated sequence [18,19] and obeys $\mathbf{p}=0$, there is no extra attenuation when the motion remains coherent during the echo formation period. A comparison of PGSTE and Double PGSTE results for otherwise identical conditions will therefore provide a tool for identifying the relative contribution of stationary random flow in the system.

In contrast, pseudodiffusion measured by PGSTE, with $\tau_c^u \ll \Delta$, results in an effective diffusion coefficient independent of observation time,

$$D_{\text{eff}} = \overline{u_z^2}\tau_c^u = \frac{1}{3}\overline{u^2}\tau_c^u \quad (7)$$

The pseudodiffusion attenuation will *not* be refocused by the Double PGSTE sequence [8]. Both the intermediate case when $\Delta \sim \tau_c^u$, and a situation, where due to, for instance, spatial heterogeneity, the system is characterised by a range of correlation times so that $\tau_{c,\min}^u < \Delta < \tau_{c,\max}^u$, a partial refocusing will occur in the Double PGSTE sequence.

4. Evolution of the effective diffusion coefficients

Under the conditions described in the experimental section, the H_2O_2 decomposition in the presence of the catalyst particle doped with Cu was monitored via the effective diffusion coefficient. We performed the experiments in both *z*- and *x*-direction alternated during one uninterrupted decomposition reaction. The whole experiments consisted of a series of $D_{\text{eff}}^z - D_{\text{eff}}^x - D_{\text{eff}}^z - D_{\text{eff}}^x \ldots$ measurements, using the PGSTE sequence (Fig. 3A) with $\Delta = 45$ ms, equal for both directions. Fig. 4A shows the results for a total reaction time of almost 17 h. The quotient D_{eff}/D_0 for both directions is plotted vs. t_r, where D_0 represents the isotropic diffusion coefficient measured in water in the presence of the same catalyst particle, i.e. the condition expected at the end of the reaction.

The reaction begins with values more than two orders of magnitude larger in *z*- and about one order of magnitude larger in *x*-direction, compared to free isotropic self-diffusion. During approximately 9 h, the decay follows a rather regular behaviour, where the reaction rate at the catalyst sites is sufficiently high to produce bubbles continuously, which perturb the liquid and enhance the transport of H_2O_2 molecules to the pellet. Notice that the values in both directions follow the same trend during that period. At $t_r \approx 8.8$ h, the *x*-component is close to the self-diffusion value (i.e. $D_{\text{eff}}^x/D_0 \sim 1$) which means that from this point on, the rate of reaction is too low to generate a noticeable effect on D_{eff}^x. At the same time, the component D_{eff}^z also begins to decrease sharply as is seen from the change of the slope of the upper curve in Fig. 4. A probable explanation for this qualitative change is a significant reduction in bubble rate and/or size once oxygen generation falls below a critical threshold. In this context, little bubbles generated by extremely low reaction rates could give minor

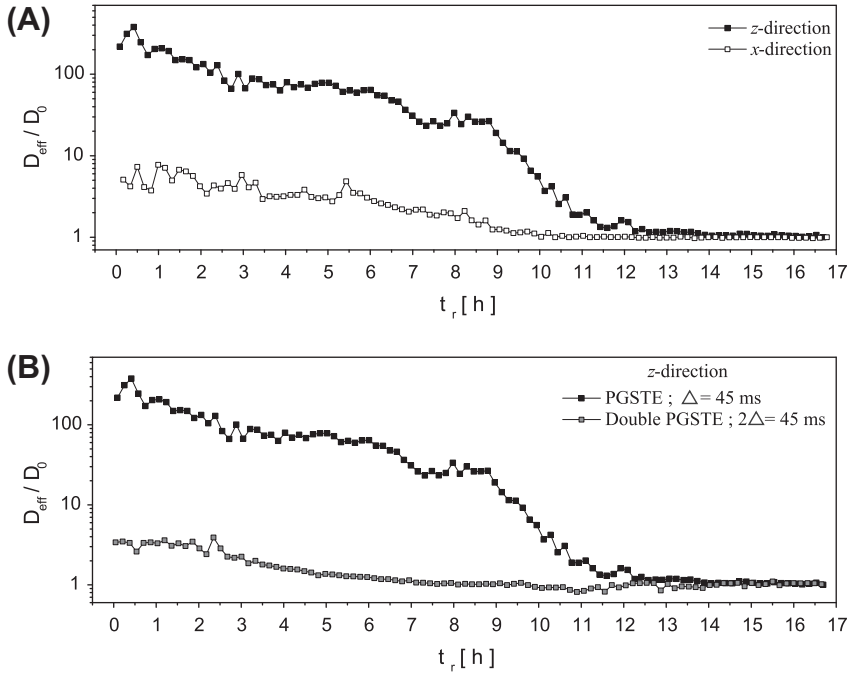

Fig. 4. (A) Evolution of the effective diffusion coefficient (normalized by the molecular diffusion coefficient), D_{eff}/D_0 in z- and x-direction vs. reaction time. An H_2O_2 decomposition catalysed by a pellet doped with Cu was monitored during ~17 h by a PGSTE sequence, with observation time Δ = 45 ms. (B) Comparison with results from PGSTE and Double PGSTE with the same observation time, Δ = 45 ms.

contributions to an increase of the bulk self-diffusion coefficient. The possibility of observing these perturbations by means of the effective diffusion coefficient will depend on the sensitivity of the sequence to motion, i.e. essentially the proper choice of the observation interval Δ. At about t_r = 14 h, where both components coalesce in the unique isotropic self-diffusion value, the reaction has essentially ceased.

In order to check the viability of modelling the liquid motion by a stationary random flow scheme, we made use of the Double PGSTE sequence. As mentioned in the previous section, a Double PGSTE sequence (Fig. 3B) must refocus the random contribution from the bubbles (the term related with **u**) when the liquid is in the stationary random flow regime. As a result we should only observe contributions from isotropic self-diffusion and from parts of the liquid undergoing pseudo-diffusion.

A set of experiments were performed in the same sample and for identical conditions as presented above, but instead using the Double PGSTE. The experiments were also carried out in both z- and x-direction alternating during one uninterrupted decomposition reaction. For direct comparisons with the previous measurements, as the sequence has two periods of evolution of duration Δ, those values were chosen such that $2\Delta_{Double} = \Delta_{PGSTE}$. For the sake of clarity, however, in what follows we will refer to the observation time. The number of points for every single realization was set such that the temporal resolution during the reaction is the same as that in the reaction monitored with the PGSTE (see Experimental section).

Fig. 4B shows D^z_{eff}/D_0 obtained with 45 ms observation time by using either PGSTE or Double PGSTE. The difference between both methods is remarkable. Although no total cancellation of the extra contribution is observed, as predicted by a random flow situation, the values are almost two orders of magnitude smaller in the data obtained with the Double PGSTE sequence. This means that almost the whole volume of liquid experiences random velocities with a correlation time much larger than the observation time, while a very small fraction possesses random motion with correlation times shorter than 45 ms. It is noteworthy that close to the time where the PGSTE data show a break, the Double PGSTE is completely effective in refocusing the extra contributions (only self diffusion remains), consistent with the fact that the bubble generation rate becomes very low.

There is, however, another feature of the stationary random flow regime that can directly be investigated by the PGSTE sequence: its dependence on the observation time. As was outlined above, variation of the observation time serves two purposes. On one hand, it provides a means to distinguish between stationary random flow and pseudodiffusion. On the other hand, it is equivalent to varying the time scale relative to the correlation times τ^u_c and τ^r_c and thus test the validity of the conditions discussed after Eq. (3). Experiments with different observation times were carried out in order to explicitly observe the relation between D^z_{eff} and Δ. Three independent decomposition reactions were monitored for about 17 h each (different total t_r for different experiments) with Δ = 90, 45, and 10 ms. Fig. 5A shows the time evolution of D^z_{eff}/D_0 for the different values of Δ. The same set of data in x-direction (data not shown) follows a similar behaviour, with correspondingly much smaller values. During the first 6 h, the three curves follow a similar trend. The quotient D^z_{eff}/D_0 vs. Δ for different reaction times during this period is presented in Fig. 5B. The solid lines represent linear fittings, to highlight the consistency with Eq. (6). This equation states that the slope is a fraction of the mean-squared random velocity, $\overline{u^2}$. This effect is also observed in the linear fits of Fig. 5B, where the slopes decrease with time because when the decomposition proceeds, the mean velocity of the liquid driven by the bubbles decreases accordingly.

At certain time of the reaction the number, or the size, of formed bubbles becomes small, suggesting that care has to be taken from that time onwards in modelling the liquid motion as random flow. The sensitivity of the pulse sequence to motion (i.e. the observation time), starts playing an important role. The effective diffusion coefficient values will certainly depend on Δ, because

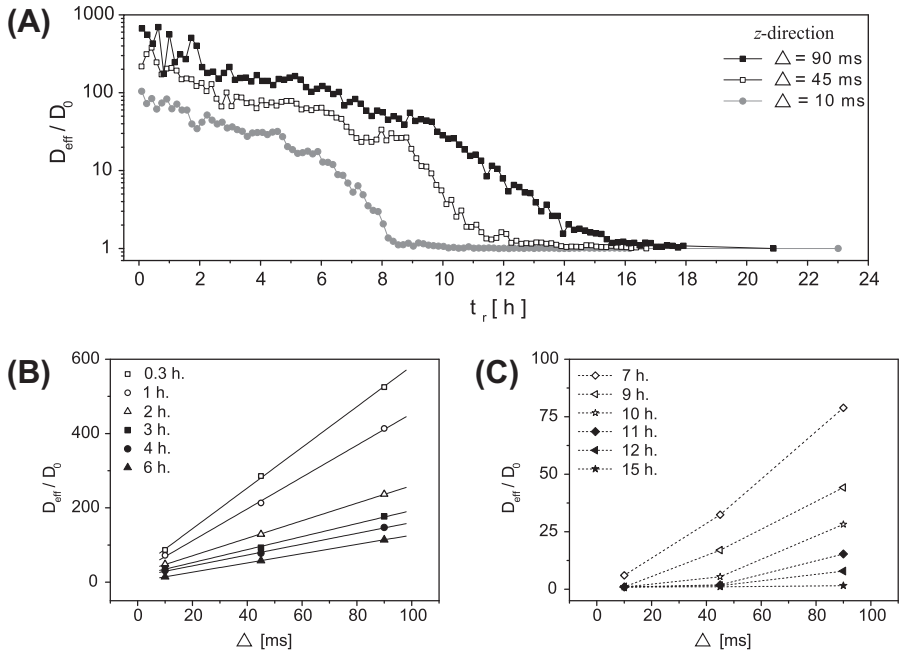

Fig. 5. (A) D^z_{eff}/D_0 vs. reaction time, obtained with a PGSTE sequence in the same conditions presented in previous plots, Δ = 90, 45 and 10 ms. (B) D^z_{eff}/D_0 vs. Δ, corresponding to different stages of the reaction curves shown in (A), in the interval between 20 and 320 min after the reaction has started. The lines are linear fits. The decrease in the slopes with increasing time is related to the drop of the mean-squared velocities of the liquid molecules ($\overline{u^2}$) produced by the gas bubbles. (C) The same plot as (B), in this case for t_r between 420 and 900 min. The effective diffusion coefficient no longer varies linearly with Δ. The same plot as (B), in this case for t_r between. The effective diffusion coefficient no longer varies linearly with.

the longer Δ allows for a larger mean-squared displacements of the molecules; this will, however, not necessarily follow a linear behaviour of D_{eff} as predicted by Eq. (6) which only takes into account the fraction of molecules involved in stationary random flow. Fig. 5C shows D^z_{eff}/D_0 vs. Δ for t_r between 7 and 15 h after the beginning of the reaction. The relation between the effective diffusion coefficient and the observation time is clearly no longer linear. At decreasing D_{eff}, the constant contribution of self-diffusion becomes more important. The mean-squared displacement of spins, the actual quantity measured by the PGSTE sequence, can be expressed as

$$\overline{Z^2} = 2\Delta\left[D_0 + \frac{1}{6}\overline{u^2}\Delta\right] \tag{8}$$

where self-diffusion was supposed to be in 1 dimension (in this case in z – direction) and pseudodiffusion contribution is not considered. The second term will, for a $\overline{u^2}$ that decreases with reaction time as a consequence of reduced bubble generation, become on the order of D_0, first for small Δ, then, at later reaction stage, for larger Δ. This explains the fact that the stronger decay in D_{eff}/D_0 occurs at ever increasing reaction times for longer observation times chosen in the experiments (Fig. 5A).

In other words, during a long period of time the rate of mass transport to the catalyst, enhanced by the rising bubbles, is much larger than the rate of H_2O_2 reaction at the sites. Consequently, the concentration decreases together with the effective diffusion coefficient following a regular trend. This is the period of time, where the liquid can be described by a stationary random flow scheme. However, at a certain concentration value, or equivalently at a certain rate of bubble production, the rate of reaction at the metal sites and the mass transport rate become comparable. Then, fewer and smaller bubbles are being produced and the effective diffusion coefficient decreases. This effect is observed at different reaction times depending on the Δ value used. The longer the observation time, the smaller the perturbations that the sequence is able to reflect into the echo decay.

5. Comparing different catalyst particles

In order to illustrate the use of the effective diffusion coefficient evolution curves in a practical application, we performed experiments with two different catalyst particles. The same total amount of liquid, as well as initial H_2O_2 concentration and pulse sequence parameters were used in a decomposition catalyzed by both cylindrical pellets, one doped with Cu and the other by Pt, the latter being the more effective.

Fig. 6 shows the evolution of D^z_{eff}/D_0 as the reaction progresses, for both samples, obtained by PGSTE experiments with Δ = 45 ms. The curve corresponding to the Pt-doped sample presents much larger initial values (about one order of magnitude) compared to the Cu pellet. For the Pt-doped pellet, the effective diffusion coefficients rapidly decrease with time t_r. Five hours after the reaction started, there is a change in the slope associated with a drop in the rate of bubble generation and decomposition. In this case, due to the higher rate of decomposition at the Pt sites compared to the Cu-pellet, it can be assumed that diffusion itself is never sufficient to dissolve the extra oxygen generated in the pore space and bubbles are always present. The reaction never becomes diffusion controlled. Hence, the pronounced decrease of D^z_{eff}/D_0 as in the Cu case, is not observed here. Finally, the effective diffusion coefficient reaches the expected value at circa 9 h for the Pt-pellet, in contrast with 14 h for the Cu-pellet when the available amount of H_2O_2 is completely decomposed. For directly comparable pellets with only one variable altered, such as pore size, coking degree and metal content, the temporal evolution and the absolute value of the ratio D_{eff}/D_0 can provide a simple access to the reaction efficiency of a single pellet. Further discussions about the analysis of the curves is beyond the scope of this article.

6. Discussions and conclusions

In this work, we employed pulsed field gradient NMR methods to obtain parameters of fluid motion in a closed volume around a

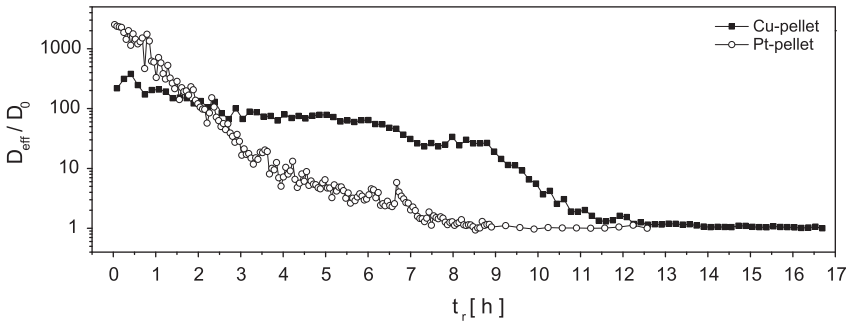

Fig. 6. Comparison of D^{z}_{eff}/D_0 vs. reaction time with Cu- and Pt-doped catalyst particles obtained by PGSTE sequence with Δ = 45 ms for the decomposition of H_2O_2.

single pellet containing catalytically active material. The determination of the effective diffusion coefficient from the initial, low-q data of a single PGSTE experiment, makes the evolution of the overall liquid motion, and thus the reaction progress, readily available. A compensated technique employing four pulsed field gradients separated the relative contributions of coherent motion during the observation interval, i.e. stationary random flow, from pseudodiffusive processes. For the system of H_2O_2 decomposition, pseudodiffusion plays a minor role for observation times in the range 10–90 ms, indicating that fluid transport predominantly takes place along straight trajectories during this period, a notion that is supported by the picture of fluid transport being dominated by rising oxygen bubbles carrying the solution with them. The method can thus also be used for estimating correlation times and lengths in a more complex geometry.

The concept of estimating reactor efficiency via fluid motion possesses some advantages over alternative approaches. Using NMR, spectroscopic information is often not available in a structured medium, in particular in the presence of metal containing particles [20] and relaxation times show no direct dependence on reactant concentration. The identification of temperature as a further parameter being linked with reaction progress has been demonstrated [21,22], but depends on large temperature differences or requires insertion of specific temperature-sensitive objects. Non-NMR methods, on the other hand, frequently rely on optically transparent sample walls and, in the case of monolith and fixed bed reactors, are severely limited by the interfering interfaces.

While we demonstrate here the feasibility of the approach for H_2O_2 decomposition, the concept can doubtless be extended towards other gas-forming reactions, and also to a wide class of other reactions, where the exothermic signature leads to an increase in fluid motion due to convection.

The aim of this work was to present an easily accessible quantity that can serve as a probe of reaction efficiency and its time dependence. It has not been the purpose to objectively quantify reaction rates and conversion rates, a task that, subject to suitable calibrations, can possibly be achieved. For instance, the gas and heat production rates are directly linked with reaction progress and both affect the transport of fluid molecules which can be estimated based on an energy balance approach.

The best performance of the presented method is expected for assessing and comparing reactor pellets during different stages of modification, such as coking/regeneration, surface treatment, metal impregnation, or as a means to provide quality control during lifetime monitoring. While the single PGSTE experiment gives adequate information about the evolution of the relative reactor performance, a combination with Double PGSTE and variation of displacement direction as well as observation time allows a more thorough understanding of the actual diffusion and convection processes involved. It is important to note that, by the very nature of the double PGSTE method, the same data can straightforwardly be acquired under realistic flow conditions, where the contribution due to coherent transport is simply filtered out, provided the observation times are chosen suitably. These times can be varied over a rather broad range; depending on other critical parameters such as relaxation times and on the required precision, the acquisition time of the methods can be reduced by at least one order of magnitude, allowing access to much quicker reaction processes than those investigated in this study. An extension towards a spatially resolved method is feasible and makes possible the visualization of the distribution of regions of high and low reactivity within a fixed bed or trickle bed reactor column [23]. Finally, the proposed experiments can be carried out without any hardware modifications on any low magnetic field desktop devices equipped with pulsed field gradients, making routine assessment of catalytically active pellets available immediately after the production or treatment process.

7. Experimental Section

In this work, we focus on the reaction $2H_2O_2$ (liquid) → $2H_2O$ (liquid) + O_2 (gas) in the presence of two different catalyst particles. The setup consisted of a single catalyst pellet immersed in a 7 mm inner diameter tube, filled with 1.1 ml of 5% v/v H_2O_2 aqueous solution. All the experiments presented here were performed in a Bruker DSX200 spectrometer equipped with a 10 mm birdcage, r.f. coil. The device operates at 200 MHz ^{1}H Larmor frequency. The applied magnetic field gradients were aligned either along the axis of gravity, parallel to the external magnetic field and labelled as z-direction here, or perpendicular to that axis, labelled as x-direction. Two different catalyst particles were used, (i) a cylindrical pellet with 4 mm diameter and 4 mm height, the matrix being made of Al_2O_3, with Cu as catalytically active sites (Bayer CH-FCH-RD Geb. 8, Cu cont. 51.2% weight) and (ii) a cylindrical pellet with 3 mm diameter and 3 mm height, made of Al_2O_3, with Pt as catalytically active sites (Company Alfa Aesar).

The aqueous hydrogen peroxide solutions were obtained by mixing distilled water (CHROMASOLV Plus, Sigma-Aldrich), with hydrogen peroxide aqueous solution 30% by weight (Riedel –deHaen). The different reaction experiments were monitored for several hours without any further hydrogen peroxide supply. In all cases the tube was placed into the coil in a position centred in the sensitive volume close to the pellet, as shown in Fig. 1 (the amount of liquid placed in the sensitive volume of the coil was estimated to be 0.3 ml). Therefore, the NMR signal results from the liquid at maximum 5 mm from the catalyst outer surface. In order to allow comparison between different realizations, the amount of liquid and initial concentrations were kept constant. A stimmulated echo of the PGSE and Double PGSE was used to allow for variable observation times since T_2 could be considerably

shorter than T_1. This is certainly the case of H_2O_2 aqueous solutions, where at 200 MHz Larmor frequency, $T_1 \sim 3$ s, whereas T_2 covers a wide range from 10 ms to 3 s depending on concentration and pH value [5,24]. Fig. 3 shows the pulse sequences used in this work, (A) PGSTE and (B) Double PGSTE [8].

When employing the PGSTE pulse sequence, we set the observation times to either $\Delta = 90$, 45 or 10 ms, always equal for both directions, with $\delta = 1$ ms and 20 gradient steps, with four scans per step. Each individual experiment took 2.5 min. During the experiments performed in z-direction for different observation times, $\Delta = 90$, 45 and 10 ms, different pulsed field gradient durations were employed in order to ensure a comparable signal decay within the range of available gradient strengths: for the last two cases, $\delta = 1$ ms, while for $\Delta = 90$ ms, $\delta = 500$ μs was used.

For the experiments with Double PGSTE (Fig. 3B), as the sequence contains two periods of evolution of duration Δ, we set the values such that $2\Delta_{\text{Double}} = \Delta_{\text{PGSTE}}$, to make possible a direct comparison between results. The length of the pulse gradients was set to be $\delta = 500$ μs. Since the phase cycling for this sequence requires 8 scans [25], only 10 gradient steps were acquired, to keep the acquisition time for individual experiments equal to those performed with a PGSTE sequence, 2.5 min. Thus, the temporal resolution during the reaction is the same in both set of experiments.

Acknowledgments

The authors are grateful to T. Oehmichen and L. Datsevich for providing and preparing the samples and for fruitful discussions within the reaction part of this work. The authors appreciate as well the discussions and ideas provided by F. Casanova. Financial support from Deutsche Forschungsgemeinschaft DFG (Sta 511/6) is gratefully acknowledged.

References

[1] O. Levenspiel, Chemical Reaction Engineering, John Wiley & Sons, 1999.
[2] X. Ren, S. Stapf, B. Blümich, Multiscale approach to catalyst design, in: S. Stapf, S. Han (Eds.), Nuclear Magnetic Resonance Imaging in Chemical Engineering, Wiley-VCH Verlag GmbH & Co., KGaA, 2006. (Chapter 3).
[3] A. Amar, L. Buljubasich, B. Blümich, S. Stapf, Transport properties in small-scale reaction units, in: S. Codd, J.D. Seymour (Eds.), Magnetic Resonance Microscopy: Spatially Resolved NMR Techniques and Applications, Wiley-VCH, Wiley-VCH Verlag GmbH & Co., KGaA, 2008. (Chapter 16).
[4] A.V. Matveev, L.V. Barysheva, I.V. Koptyug, V.M. Khanaev, A.S. Noskov, Investigation of fine granular material flow through a packed bed, Chem. Eng. Sci. 61 (2006) 2394–2406.
[5] L. Buljubasich, B. Blümich, S. Stapf, Quantification of H_2O_2 concentrations in aqueous solutions by means of combined NMR and pH measurements, Phys. Chem. Chem. Phys. 12 (2010) 13166–13173.
[6] L.B. Datsevich, Some theoretical aspects of catalyst behaviour in a catalyst particle at liquid (liquid–gas) reactions with gas production: oscillation motion in the catalyst pores, Appl. Catal. A 247 (2003) 101–111.
[7] L.B. Datsevich, Oscillation theory. Part 4. Some dynamic peculiarities of motion in catalyst pores, Appl. Catal. A 294 (2005) 22–33.
[8] P. Callaghan, Principles of Nuclear Magnetic Resonance Microscopy, Clarendon Press, Oxford, 1991.
[9] J. Kärger, W. Heink, The propagator representation of molecular-transport in microporous crystallites, J. Magn. Reson. 51 (1983) 1–7.
[10] P.J. Basser, J. Mattiello, D. LeBihan, MR diffusion tensor spectroscopy and imaging, Biophys. J. 66 (1994) 259–267.
[11] J.J. Tessier, K.J. Packer, The characterization of multiphase fluid transport in a porous solid by pulsed gradient stimulated echo nuclear magnetic resonance, Phys. Fluids 10 (1998) 75–85.
[12] K.J. Packer, S. Stapf, J.J. Tessier, R.A. Damion, The characterisation of fluid transport in porous solids by means of pulsed magnetic field gradient NMR, Magn. Reson. Imag. 16 (1998) 463–469.
[13] A. Amar, S. Stapf, B. Blümich, Internal fluid dynamics in levitated drops by fast magnetic resonance velocimetry, Phys. Rev. E 72 (2005) 030201.
[14] S. Harms, S. Stapf, B. Blümich, Application of k-space and q-space encoding NMR techniques on granular media in a 3D model fluidised bed reactor, J. Magn. Reson. 178 (2006) 308–317.
[15] E.O. Stejskal, J.E. Tanner, Spin diffusion measurements-spin echoes in presence of a time-dependent field gradient, J. Chem. Phys. 42 (1965) 288–292.
[16] P.T. Callaghan, S.L. Codd, J.D. Seymour, Spatial coherence phenomena arising from translational spin motion in gradient spin echo experiments, Concepts Magn. Reson. 11 (1999) 181–202.
[17] O. Nalcioglu, Z.H. Cho, Measurement of bulk and random directional velocity fields by NMR imaging, IEEE Trans. Med. Imag. MI-6 (1987) 356–359.
[18] P.T. Callaghan, Y. Xia, Velocity and diffusion imaging in dynamics NMR microscopy, J. Magn. Reson. 91 (1991) 326–352.
[19] A. Caprihan, J.D. Seymour, Correlation time and diffusion coefficient imaging: application to a granular flow system, J. Magn. Reson. 144 (2000) 96–107.
[20] M. Küppers, C. Heine, S. Han, S. Stapf, B. Blümich, In-situ observation of diffusion and reaction dynamics in gel microreactors by chemically resolved NMR microscopy, Appl. Magn. Reson. 22 (2002) 235–246.
[21] L.F. Gladden, F.J.R. Abegao, C.P. Dunckley, D.J. Holland, M.H. Sankey, A.J. Sederman, MRI: operando measurements of temperature, hydrodynamics and local reaction rate in a heterogeneous catalytic reactor, Catal. Today 155 (2010) 157–163.
[22] I.V. Koptyug, A.V. Khomichev, A.A. Lysova, R.Z. Sagdeev, Spatially resolved NMR thermometry of an operating fixed-bed catalytic reactor, J. Am. Chem. Soc. 130 (2008) 10452.
[23] B.S. Akpa, M.D. Mantle, A.J. Sederman, L. Gladden, In situ C-13 DEPT-MRI as a tool to spatially resolve chemical conversion and selectivity of a heterogeneous catalytic reaction occurring in a fixed-bed reactor, Chem. Commun. 21 (2005) 2741–2743.
[24] L. Buljubasich, B. Blümich, S. Stapf, Reaction monitoring of hydrogen peroxide decomposition by NMR relaxometry, Chem. Eng. Sci. 65 (2010) 1394–1399.
[25] A. Jerschow, N. Müller, Suppression of convection artifacts in stimulated-echo diffusion experiments. Double-stimulated-echo experiments, J. Magn. Res. 125 (1997) 372–375.